Planar triple-decker and capped octahedral clusters of group-6 transition metals

Ranjit Bag, Sourav Gayen, Stutee Mohapatra, P.K. Sudhadevi Antharjanam, Jean-François Halet, Sundargopal Ghosh

Planar triple-decker and capped octahedral clusters of group-6 transition metals

Ranjit Bag,[a] Sourav Gayen,[a] Stutee Mohapatra,[a] P. K. Sudhadevi Antharjanam,[b] Jean-François Halet,*[c] and Sundargopal Ghosh*[a]

[a] *Department of Chemistry, Indian Institute of Technology Madras, Chennai 600 036, India*

[b] *SAIF, Indian Institute of Technology Madras, Chennai 600 036, India*

[c] *CNRS–Saint-Gobain–NIMS, IRL 3629, Laboratory for Innovative Key Materials and Structures (LINK), National Institute for Materials Science (NIMS), Tsukuba, 305-0044, Japan*

E-mail: jean-francois.halet@univ-rennes1.fr (J.-F. Halet), sghosh@iitm.ac.in (S. Ghosh).

Dedicated to Professor Pradeep Mathur on the occasion of his 65th birthday in recognition of his outstanding contributions in the area of organometallic chemistry

Keywords: cobalt, metallaborane, octahedral cluster, triple-decker, tungsten

ABSTRACT

Recent isolation and structural characterization of a planar triple-decker metallaborane complex of tungsten prompted us to synthesize its molybdenum analogue. Therefore, we have explored the thermolysis reaction of the intermediates obtained from the low-temperature reaction of [Cp*$MoCl_4$] (Cp* = η^5-C_5Me_5) and $LiBH_4$ with $Co_2(CO)_8$. The reaction indeed produced the analogous triple-decker complex of molybdenum with a planar middle-deck [$(Cp^*Mo)_2\{\mu$-η^6:η^6-$B_4H_4Co_2(CO)_5\}(H)_2$], **1**, along with the formation of the reported [$(Cp^*Mo)_2B_5H_9$] metallaborane. In an effort to isolate multi-decker complexes with a different geometries, we have also further explored the thermolysis reaction of the intermediates obtained from the low-temperature reaction of [Cp*WCl_4] and $LiBH_4$ with $Co_2(CO)_8$. The reaction afforded an octahedral cluster, [$\{Cp^*W(CO)_2\}_2(\mu$-$H)_2B_3H_3Co_2(CO)_4$], **2**, along with the formation of the bimetallic cluster [$(Cp^*W)_2B_3H_3(\mu$-$H)_2Co_2(CO)_4(\mu$-$CO)_2$], **3**. The cage geometry of compound **2** is based on an octahedron with one additional vertex capping a trigonal face. That of compound **3** is a bicapped trigonal-bipyramidal analogue to the parent compound [$(Cp^*W)_2B_5H_9$]. While compound **1** has been characterized by various spectroscopic analyses, compounds **2** and **3** have been characterized by multiple spectroscopic and single-crystal X-ray diffraction analyses. Density-functional theory (DFT) calculations account for their stability and structural variation.

1. Introduction

The discovery of ferrocene[1] augmented the field of metal sandwich compounds that have become the icon of modern organometallic chemistry.[2] Because of the enormous use of sandwich compounds,[3,4] research was extended to multi-decker systems. Among them, triple-decker

complexes of transition metals are well known.[5-8] They have a unique structure in which two metal atoms are located between three cyclic frameworks. The very first transition metal triple-decker sandwich complex tris(cyclopentadienyl) di-nickel cation $[CpNi(\mu\text{-}\eta\text{:}\eta\text{-}Cp)NiCp]^+$ was reported by Werner and Salzer in 1972.[9] However the first air-stable and neutral triple-decker metallacarborane compound, namely $[RC_2B_3H_4(CpCo)_2]$ (R =H/Me) was reported by Grimes.[10] Apart from the structural diversity, triple-decker complexes have several applications in metal-complex catalysis,[11] hydrogen storage,[12] and molecular electronics[13].

During the course of our studies on triple-decker complexes, we have isolated a few such triple-decker complexes containing a puckered or a planar borane/heteroborane middle-deck.[14-16] In our early communication, the characterization of a unique example of poly-metallic 24-valence-electron (ve) tungsten triple-decker sandwich complexes with puckered or planar middle-decks comprising bridging hydrogen atoms prompted us to synthesize the analogous triple-decker complex of molybdenum.[17] Therefore, we have explored the thermolysis reaction of the intermediates obtained from the low-temperature reaction of $[Cp^*MoCl_4]$ and $LiBH_4$ with $Co_2(CO)_8$. Further, we have revisited the thermolysis reaction of the intermediates obtained from the reaction of $[Cp^*WCl_4]$ and $LiBH_4$ with $Co_2(CO)_8$ aiming to synthesize other triple-decker complexes with a different geometry. The main results are reported here.

2. Results and discussion

The thermolysis reaction of an *in situ* produced intermediate, obtained from the low-temperature reaction of $[Cp^*MoCl_4]$ and $LiBH_4$ with $Co_2(CO)_8$ was carried out similarly to that we performed earlier with Cp^*WCl_4.[17] The reaction indeed yielded a triple-decker sandwich complex of molybdenum $[(Cp^*Mo)_2\{\mu\text{-}\eta^6\text{:}\eta^6\text{-}B_4H_4Co_2(CO)_5\}(\mu\text{-}H)_2]$, **1**, along with known

$[(Cp^*Mo)_2 B_5H_9]$[18] (Scheme 1). Note that this reaction also produced some low yielded air and moisture sensitive compounds which we were unable to isolate and characterized. Preparative thin-layer chromatography was used for the separation of the comparatively stable **1** and $[(Cp^*Mo)_2B_5H_9]$, which allows the characterization of the pure species. The detailed spectral characterization of **1** is discussed below.

(Scheme 1 near here)

Compound **1** was isolated as a brown solid in 15% yield. The ESI-MS of **1** showed a molecular ion peak at *m/z* = 774.9767. Its $^{11}B\{^1H\}$ NMR spectrum of **1** showed two signals at δ = 103.8 and 50.9 ppm indicating the existence of two different types of boron atoms. Along with the signals for B-H_t protons at δ = 6.44 and 3.13 ppm, the ^1H NMR spectrum shows two types of Cp* ligands at δ = 2.01 and 1.87 ppm. In addition, an up-field chemical shift at δ = -11.24 ppm observes in the ^1H NMR spectrum which is due to the presence of two Mo-*H*-B protons. The ^{13}C NMR spectrum also verified the existence of Cp* ligands. The stretching frequencies corresponding to both the terminal and bridging CO ligands, as well as the B*Ht* groups, were visible in the IR spectra. Complete characterization of **1** was performed based on the spectroscopic data in the context of the planar triple-decker complex of tungsten recently reported by us.[17] We could grow suitable crystals of **1** for X-ray analysis, but all spectroscopic data mentioned above are similar to the spectroscopic data of the reported tungsten triple-decker complex. This led us to conclude that the geometrical arrangement of **1** is iso-structural to the reported W-triple-decker sandwich complex $[(Cp^*W)_2(\mu\text{-}H)_2\{\mu\text{-}\eta^6\text{:}\eta^6\text{-}B_4H_4Co_2(CO)_5\}]$ (**I**).[17] The hexagonal $[Co_2(CO)_5B_4H_4]$ planar middle ring of the compound is sandwiched between two {Cp*Mo} units. Thus, compound **1** is a rare example of 24-ve triple-decker complex with a planar middle-deck consisting of bridging hydrogen atoms.

In parallel to the reaction described in Scheme 1, the recent isolation of planar or puckered middle-deck triple-decker complexes of tungsten prompted us to further re-explore the thermolysis reaction of the intermediates obtained from the low-temperature reaction of [Cp*WCl_4] and $LiBH_4$ with $Co_2(CO)_8$ hoping to synthesize additional triple-decker compounds with a different geometries. The reaction afforded an octahedral cluster, [{Cp*$W(CO)_2$}$_2$(μ-H)$_2$$B_3H_3Co_2(CO)_4$], **2**, a bimetallic cluster [(Cp*W)$_2$$B_3H_3$($\mu$-H)$_2$$Co_2(CO)_4$($\mu$-CO)$_2$], **3**, in addition to the reported compounds [(Cp*W)$_2$$B_5H_9$], [(Cp*W)$_2${$\mu$-$\eta^6$:$\eta^6$-$B_4H_4Co_2(CO)_5$}(μ-H)$_2$] (**I**, similar to compound **1**, see above), [(Cp*W)$_2$(μ_3-H)(μ-H)$_2$$B_4H_4Co(CO)_3$], and [{Cp*$W(CO)_2$}{Cp*W(CO)($\mu$-CO)}B($\mu$-H)$Co_2(CO)_5$] (Scheme 2).[17,19a] Preparative thin-layer chromatography was used to separate these compounds, which allows the characterization of the pure species. Below we discuss **2** and **3** in detail to characterize their spectral and structural features.

(Scheme 2 near here)

Compound **2** was isolated as a black solid in 12% yield. The ESI-MS of **2** showed a molecular ion peak at *m/z* = 1017.0198. The $^{11}B\{^1H\}$ NMR spectrum of **2** showed two signals at δ = 96.5 and 76.5 ppm, indicating the presence of two different types of boron atoms in a 1:2 ratio. In addition to the signals for B-H_t protons, the ^1H NMR spectrum shows two types of Cp* ligands at δ = 2.25 and 2.09 ppm. The ^1H NMR spectrum also shows an up-field chemical shift at δ = -5.32 ppm which is due to the presence of Co-*H*-B protons. The presence of Cp* ligands were also confirmed by ^{13}C NMR spectrum. The IR spectrum showed stretching frequencies corresponding to the CO ligands and BH_t groups. Thus, a detailed explanation eluded us until a single-crystal X-ray analysis revealed the geometry of cluster **2**.

The molecular structure of **2** shown in Fig. 1 is consistent with the spectroscopic data which indicated that the formula of **2** was [{Cp*W(CO)$_2$}$_2$(μ-H)$_2$B$_3$H$_3$Co$_2$(CO)$_4$]. Its single-crystal X-ray structure revealed that the cage geometry is based on a {WCo$_2$B$_3$} octahedron with the tungsten atom W1, cobalt atom Co2 and the two boron atoms B1 and B3 forming the equatorial plane and the B2 and Co1 atoms occupying the apical vertices. In addition, a {Cp*W(CO)$_2$} fragment caps the {Co$_2$B} triangular face. The W-Co and B-B bond length of **2** are comparable to the corresponding distances reported in other metallaboranes.[17,19] From the ^{11}B{^{1}H} NMR spectrum, the chemical shift at δ = 96.5 ppm corresponds to B3 and that at δ = 76.5 ppm corresponds to B1 and B2. ^{1}H NMR analysis identified the existence of two bridging hydrogen atoms, but crystallographically they could not be located. Therefore in order to verify their presence and position, a ^{1}H-^{11}B{^{1}H} HSQC (Heteronuclear Single Quantum Coherence) experiment was performed that established a correlation between the two bridging Co-*H*-B hydrogen atoms and the boron atom B3 with the resonance at δ = 96.5 ppm.

(Fig. 1. near here)

The existence of compound **2** allows us to draw some structural comparison with other reported monocapped-octahedral metallaborane clusters (Chart 1 and Table 1). Importantly, all the reported capped-octahedral species bear seven skeleton electron pairs (sep) as expected for mono-capped *closo*-octahedral clusters according to the cluster electron-counting rules.[20] Surprisingly enough, cluster **2** contains eight seps ({[Cp*W(CO)$_2$] 3 x 2 + [Co(CO)$_2$] 1 x 2 + [BH] 2 x 3 + [μ-H] 1 x 2} = 16/2) despite having the same mono-capped *closo*-octahedral core.[21] Note that some *closo*-octahedral clusters have been reported with eight rather than seven seps.[22]

(Chart 1 near here)

(Table 1 near here)

Compound **3** was isolated during the same reaction (Scheme 2) as a brown solid in 18% yield. The ESI-MS of **3** showed a molecular ion peak at *m/z* = 963.0439. The $^{11}B\{^{1}H\}$ NMR spectrum of **3** showed three signals at δ = 99.3, 82.5 and 25.7 ppm in a 1:1:1 ratio indicating the presence of three different types of boron environments. In addition to the signals for B-H_t protons at δ = 8.07 and 5.20 ppm, the ^{1}H NMR spectrum revealed one type of Cp* ligand at δ = 2.18 ppm. The ^{1}H NMR spectrum also showed an up-field chemical shift at δ = -13.72 ppm due to the presence of W-*H*-B protons. The presence of Cp* ligand was also confirmed by ^{13}C NMR. The IR spectrum showed stretching frequencies corresponding to both terminal and bridging CO ligands and BH_t groups. Thus, an unambiguous conclusion eluded us until a single-crystal X-ray analysis revealed the geometry of the cluster core.

(Fig. 2. near here)

As shown in Fig. 2, the molecular structure of **3** is consistent with the spectroscopic data. The asymmetric unit of the crystal structure of **3** contains two independent molecules (one, molecule B, is shown in Fig. 2) having similar geometric parameters. The structure can be viewed as an open and flattened *nido* hexagonal-bipyramid with atoms Co3, Co4, B3, B4 and B5 constituting the base capped above and below by W3 and W4, respectively. Note the latter atoms are strongly bonded. If the classical skeletal electron counting formalism[20] is applied, cluster **3** can be viewed

as electron deficient 6-sep *oblato-nido*-species derived from an 8-vertex *oblato-closo* hexagonal bipyramidal cluster with a short cross-cluster M-M bond (2.871 Å). It is somewhat longer than that experimentally measured in $[(Cp^*W)_2\{\mu\text{-}\eta^6\text{:}\eta^6\text{-}B_4H_4Co_2(CO)_5\}(\mu\text{-}H)_2]$ (**I**) which is 2.790 Å long.[17] Indeed, compound **3** is structurally and electronically analogous to other hypoelectronic metallaboranes[24] such as $[(Cp^*W)_2B_5H_5(\mu\text{-}H)_4]$ or $[(Cp^*Cr)_2Co(CO)_3B_4H_7]$ reported by Fehlner *et al.*,[19,25a] and the tungstaboranes $[(Cp^*W)_2M(CO)_4B_4H_8]$ (M = W, Mo, and Cr) reported recently by us.[25d] Note that the W-W and B-B bond lengths of **3** are comparable to the bond lengths measured in $[(Cp^*W)_2(\mu\text{-}H)_4B_5H_5]$[19] and others (Table 2).

(Table 2 near here)

To get insight into the electronic structure of the novel molecules reported here, density functional theory (DFT)-based quantum chemical calculations were carried out on simplified models **I'**, **1'**, and **3'**, Cp analogs of **I**, **1**, and **3**, respectively. The geometry optimization resulted in bond distances and angles that agree rather well with the solid-state structural parameters was noted (Table S1). As expected from the spectroscopic data obtained for **1** (*vide supra*), the optimized structure of **1'** corresponds to a dimolybdenum triple-decker sandwich complex where the hexagonal planar $[B_4H_4Co_2(CO)_5]$ middle-deck is sandwiched between two {Cp*Mo} fragments (Fig. 3). Indeed, cluster **1'** is analogous to the 6-sep *oblato-closo* triple-decker clusters $[(Cp^*W)_2\{\mu\text{-}\eta^6\text{:}\eta^6\text{-}B_4H_4Co_2(CO)_5\}(\mu\text{-}H)_2]$ (**I**),[17] or $[(Cp^*Re)_2\{\mu\text{-}\eta^6\text{:}\eta^6\text{-}B_4H_4Co_2(CO)_5\}]$,[26] characterized by high metal coordination numbers, a rather short Mo-Mo cross-cluster distance (2.783 Å), and a formal cluster electron count three seps short of that required for a canonical *closo*-structure of the same nuclearity.[27]

(Fig. 3 near here)

Stability as well as M–M bond strengths were analyzed. As expected, the W and Mo *oblato-closo* species **I'** and **1'**, show similar frontier molecular orbitals (MO) with substantial HOMO-LUMO gaps of 3.268 eV and 3.260 eV (Table S2), respectively, diagnosis of good kinetic stability. Similarly, a rather less HOMO-LUMO gap (2.982 eV) is computed for the *oblato-nido* species **3'** (Fig. 4). Analysis of the nodal properties of the HOMO and LUMO indicate strong σ- and δ-bonding interactions between the metal atoms, not only M and Co but also M and M (M = Mo, W). Strong σ-antibonding interactions between metal atoms are observed in the LUMO+3 (Fig. 4).

Wiberg bond indices (WBI)[28] were obtained from natural bond orbital (NBO) analysis.[29] Higher WBI values (Table S1) for triple-decker complexes further supported the fact that the presence of closed middle deck strengthening the M-M bond for both triple-decker complexes (**I'** and **1'**), whereas *oblato-nido* species **3'** show a weaker M-M bond. In addition, a higher M-M bond WBI value for **I'** compared to **1'** was computed.

(Fig. 4. near here)

3. Conclusion

In summary, we have described the synthesis and the spectroscopic characterization of the novel planar triple-decker complex of molybdenum $[(Cp^*Mo)_2\{\mu\text{-}\eta^6\text{:}\eta^6\text{-}B_4H_4Co_2(CO)_5\}(\mu\text{-}H)_2]$. Further, revisiting the thermolysis reaction of the intermediates obtained from the low-temperature reaction of $[Cp^*MoCl_4]$ and $LiBH_4$ with $Co_2(CO)_8$, we have successfully

synthesized and characterized two new tungsten metallaborane clusters, namely [{Cp*W(CO)$_2$}$_2$(μ-H)$_2$B$_3$H$_3$Co$_2$(CO)$_4$] and [(Cp*W)$_2$B$_3$H$_3$(μ-H)$_2$Co$_2$(CO)$_4$(μ-CO)$_2$]. Theoretical computations on the Cp analogue of [(Cp*Mo)$_2${μ-η^6:η^6-B$_4$H$_4$Co$_2$(CO)$_5$}(μ-H)$_2$] indicate that its cluster core adopts a flattened hexagonal bipyramidal geometry analogous to that encountered for the 6-sep *oblato-closo* triple-decker clusters [(Cp*W)$_2${μ-η^6:η^6-B$_4$H$_4$Co$_2$(CO)$_5$}(μ-H)$_2$] previously reported. X-ray data shows that the cage geometry of [{Cp*W(CO)$_2$}$_2$(μ-H)$_2$B$_3$H$_3$Co$_2$(CO)$_4$] is based on an octahedron with one additional vertex capping a trigonal face. The geometry of compound **3** is bicapped trigonal-bipyramidal analogue to the flattened *oblato-nido* parent [(Cp*W)$_2$B$_5$H$_9$]. These results exemplify the possibility of the synthesis of novel poly-metallic molecular clusters with original geometry and bonding from thermolysis reactions.

4. Experimental section

General procedures and instrumentation. All the experiments were performed under a dry argon atmosphere or in vacuo of using a standard glovebox or Schlenk line techniques. Compounds [Cp*MCl$_4$] (M = W and Mo) were synthesized following the method reported in the literature,[30] While other chemicals such as Cp*H, *n*-BuLi, [LiBH$_4$.thf] 2.0 M in THF, and [Co$_2$(CO)$_8$] were obtained commercially (Aldrich) and used as received. Prior to use solvents (toluene, hexane, THF) were purified by distillation from suitable drying agents (sodium/benzophenone) under dry argon. Using the three freeze-pump-thaw cycles CDCl$_3$ and C$_6$D$_6$ were degassed and stored over molecular sieves. MeI was purchased from Aldrich and freshly distilled prior to use. The external reference for the ^{11}B NMR, [Bu$_4$N][B$_3$H$_8$] was synthesized following the literature method.[31] Preparative thin-layer chromatography was performed with Merck 105554 TLC silica gel 60 F$_{254}$, layer thickness 250 µm on aluminum

sheets (20 x 20 cm). 500 MHz Bruker FT-NMR spectrometer was used to record the NMR spectra. The residual solvent protons were used as reference (δ, ppm, d_6-benzene, 7.16, $CDCl_3$, 7.26), while a sealed tube containing $[Bu_4N][B_3H_8]$ in d_6-benzene (δ_B, ppm, –30.07) was used as an external reference for the ^{11}B NMR. The infrared spectra were recorded on a JASCO FT/IR-4100 spectrometer in CH_2Cl_2 solvent. Electrospray mass (ESI-MS) spectra were recorded on an Agilent 6545 Q-TOF LC/MS instrument.

Synthesis of 1: In a flame-dried Schlenk tube [Cp*$MoCl_4$], (0.1 g, 0.27 mmol) in 10 mL of toluene was treated with a 5-fold excess of [$LiBH_4$·THF] (0.7 mL) at -78 °C and allowed to stir at room temperature for 1 h. After the removal of toluene, the residue was extracted into hexane and filtered through a frit using Celite. The brownish-green hexane extract was dried in vacuo, and taken in 10 mL of THF and heated at 60 °C in the presence of $[Co_2(CO)_8]$ (0.03 g) for 16 h. The solvent was evaporated in vacuo followed by the extraction of the residue into hexane/dcm and passing it through Celite. After removing solvent from the filtrate, the residue was subjected to chromatographic workup using silica gel TLC plates. Elution with a hexane/CH_2Cl_2 (70:30 v/v) mixture yielded brown **1** (0.014 g, 15%), $[(Cp^*Mo)_2B_5H_9]$[18] (0.017 g, 24%).

1: MS (ESI+): *m/z* calculated for $[C_{25}H_{36}O_5B_4Co_2Mo_2+H]^+$ 774.9785, found 774.9767; $^{11}B\{^1H\}$ NMR (160 MHz, $CDCl_3$, 22 °C): δ = 103.8 (s, 2B), 50.9 ppm (s, 2B); ^1H NMR (500 MHz, $CDCl_3$, 22 °C): δ = 6.44 (br, 2H, B-H_t), 3.13 (br, 2H, B-H_t), 2.01 (s, 15H, C_5Me_5), 1.87 (s, 15H, C_5Me_5), -11.24 ppm (br, 2H, Mo-*H*-B); $^{13}C\{^1H\}$ NMR (22 °C, 125 MHz, $CDCl_3$): δ = 108.5 (C_5Me_5), 107.6 (C_5Me_5), 12.6 (C_5Me_5), 12.0 ppm (C_5Me_5); IR (CH_2Cl_2, cm^{-1}): 2499, 2451 (w, BH_t), 2039, 2010, 1995, 1772 (CO).

Synthesis of 2 and **3**: In a flame-dried Schlenk tube [Cp*WCl_4], (0.1 g, 0.21 mmol) in 10 mL of toluene was treated with 5-fold excess of [$LiBH_4$·THF] (0.7 mL) at -78 °C and allowed to stir at room temperature for 1 h. After removal of toluene, the residue was extracted into hexane and filtered through a frit using Celite. The brownish-green hexane extract was dried in vacuo, and taken in 10 mL of THF and heated at 60 °C in presence of [$Co_2(CO)_8$] (0.03 g) for 16 h. The solvent was evaporated in vacuo followed by the extraction of the residue into hexane/dcm and passing it through Celite. After removal of solvent from the filtrate, the residue was subjected to chromatographic workup using silica gel TLC plates. Elution with a hexane/CH_2Cl_2 (70:30 v/v) mixture yielded black **2** (0.013 g, 12%), brown **3** (0.019 g, 18%) along with the known [$(Cp^*W)_2\{\mu\text{-}\eta^6\text{:}\eta^6\text{-}B_4H_4Co_2(CO)_5\}(H)_2$] (0.012 g, 12%), [$(Cp^*W)_2(\mu\text{-}H)_2(\mu_3\text{-}H)B_4H_4Co(CO)_3$] (0.010 g, 11%), [$\{Cp^*W(CO)_2\}\{Cp^*W(CO)(\mu\text{-}CO)\}B(\mu\text{-}H)Co_2(CO)_5$] (0.016 g, 14%) and [$(Cp^*W)_2B_5H_9$] (0.018 g, 23%).

2: MS (ESI+): *m/z* calculated for $[C_{28}H_{35}O_8B_3Co_2W_2\text{-}H]^+$ 1017.0215, found 1017.0198; $^{11}B\{^1H\}$ NMR (160 MHz, $CDCl_3$, 22 °C): δ = 96.5 (s, 1B), 76.5 ppm (s, 2B); ^1H NMR (500 MHz, $CDCl_3$, 22 °C): δ = 8.06 (br, B-H_t), 2.25 (s, 15H, $C_5\mathit{Me}_5$), 2.09 (s, 15H, $C_5\mathit{Me}_5$), -5.32 ppm (br, 2H, *Co-H*-B); $^{13}C\{^1H\}$ NMR (22 °C, 125 MHz, $CDCl_3$): δ = 102.1 (C_5Me_5), 101.0 (C_5Me_5), 11.4 ($C_5\mathit{Me}_5$), 10.6 ppm ($C_5\mathit{Me}_5$); IR (CH_2Cl_2, cm^{-1}): 2497 (w, BH_t), 2019, 1974, 1919, 1868 (CO).

3: MS (ESI+): *m/z* calculated for $[M]^+$ 963.05, found 963.0439; $^{11}B\{^1H\}$ NMR (160 MHz, $CDCl_3$, 22 °C): δ = 99.3 (s, 1B), 82.5 (s, 1B), 25.7 (s, 1B); ^1H NMR (500 MHz, $CDCl_3$, 22 °C): δ = 8.07 (br, B-H_t), 5.20 (br, B-H_t), 2.18 (s, 30H, $C_5\mathit{Me}_5$), -13.72 (br, 2H, W-*H*-B); $^{13}C\{^1H\}$ NMR (22 °C, 125 MHz, $CDCl_3$): δ = 108.1 (C_5Me_5), 12.5 ppm ($C_5\mathit{Me}_5$); IR (CH_2Cl_2, cm^{-1}): 2497, 2463 (w, BH_t), 2019, 1985, 1841, 1798 (CO).

Computational details. Optimization of all the molecules were carried out using the Gaussian 16 program.[32] Optimizations were performed employing the gradient-corrected B3LYP[33] functional along with a Def2-SVP basis set taken from EMSL (EMSL Basis Set Exchange Library. https://bse.pnl.gov/bse/portal). The model compounds were fully optimized in the gaseous state without any solvent effect starting from the coordinates obtained from X-ray crystallography. To reduce the computational effort, Cp analogues were chosen to mimic compounds **1**, **3** and **I**. Frequency calculations were carried out to check the nature of the stationary geometries and to confirm the absence of any imaginary frequency. Wiberg bond indices (WBI)[28] were obtained from a natural bond orbital analysis (NBO).[29] All the optimized structures and orbital pictures were plotted using Chemcraft (Chemcraft - Graphical Software for Visualization of Quantum Chemistry Computations. https://www.chemcraftprog.com) visualization programs. Two-dimensional electron density and Laplacian electronic distribution plots were generated using the Multiwfn package.[34]

X-ray structure determination. Suitable X-ray quality crystals of **2** and **3** were grown by slow diffusion of a hexane-CH_2Cl_2 solution. The crystal data of **2** and **3** were collected and integrated using a Bruker D8 VENTURE diffractometer with a PHOTON II detector with graphite monochromated Mo-Kα (λ = 0.71073 Å) radiation at 297(2) K. The structures were solved by dual-space algorithm using SHELXT program[35] and refined with full-matrix least-squares methods based on F^2 (SHELXL program).[36] The molecular structures were drawn using Olex2.[37] The non-hydrogen atoms were refined with anisotropic displacement parameters. Except for the bridging ones, hydrogen atoms were introduced through Fourier difference maps analysis. H atoms were finally included in their calculated positions and treated as riding on their parent

atom with constrained thermal parameters. The structure of **2** shows some disorder in the position of boron atoms over two sites with an occupancy ratio 58:42. SIMU restraints on displacement parameters were taken into account to have the same *uji* values. Crystallographic data have been deposited at the Cambridge Crystallographic Data Center as supplementary publication no CCDC-2075946(**2**), and CCDC-2075948(**3**). These data can be obtained free of charge from The Cambridge Crystallographic Data Centre via www.ccdc.cam.ac.uk/data_request/cif.

Crystal data for **2**: $C_{28}H_{33}B_3O_8W_2Co_2$, M_r = 1015.53, Monoclinic, space group $P2_1$, a = 9.345(4) Å, b = 16.737(7) Å, c = 10.656(5) Å, $\alpha = 90^\circ$, β = 100.976(14)°, $\gamma = 90^\circ$, V = 1636.1(12) Å^3, Z = 2, ρ_{calcd} = 2.061 g/cm^3, μ = 8.049 mm^{-1}, F(000) = 964, Flack parameter = 0.029(15), R_1 = 0.0272, wR_2 = 0.0618, 5647 independent reflections [$2\theta \leq 56.30^\circ$] and 411 parameters.

Crystal data for **3**: $C_{26}H_{35}B_3O_6W_2Co_2$, M_r = 961.53, Monoclinic, space group $P2_1/c$, a = 17.040(3) Å, b = 11.7667(19) Å, c = 30.210(5) Å, α = 90.000(5)°, β = 96.159(6)°, γ = 90.000(6)°, V = 6022.2(18) Å^3, Z = 8, ρ_{calcd} = 2.121 g/cm^3, μ = 8.735 mm^{-1}, F(000) = 3648, R_1 = 0.0919, wR_2 = 0.2275, 40831 independent reflections [$2\theta \leq 52.4°$] and 701 parameters.

ACKNOWLEDGMENT

The authors acknowledge the Science and Engineering Research Board (SERB) (Project No. CRG/2019/001280), New Delhi, India, for financial support. R.B and S.M thank IIT Madras for a research fellowship. S.G thanks CSIR for a research fellowship.

REFERENCES

1) T. J. Kealy, P. L. Pauson, Nature 168 (1951) 1039-1040.

2) A. F. Neto, A. C. Pelegrino, V. A. Darin, V. A. Ferrocene: 50 Years of Transition Metal Organometallic Chemistry-From Organic and Inorganic to Supramolecular Chemistry, ChemInform, 2004, p. 35.

3) (a) A. Togni, T. Hayashi, VCH, Weinheim, 1995; (b) K. Heinze, H. Lang Organometallics 32 (2013) 5623−5625.

4) E. Melendez, Inorg. Chim. Acta 393 (2012) 36−52.

5) (a) A. Haaland, Acc. Chem. Res. 12 (1979) 415-422; (b) E. D. Jemmis, A. C. Reddy, Organometallics 7 (1988) 1561−1564; (c) S. K. Ghag, M. L. Tarlton, E. A. Henle, E. M. Ochoa, A. W. Watson, L. N. Zakharov, E. J. Watson, Organometallics 32 (2013) 1851−1857.

6) (a) R. N. Grimes, R. N., Carboranes 3rd ed.; Elsevier: Amsterdam, 2016; (b) W. Siebert, J. Edwin, M. Bochmann, Angew. Chem. 90 (1978) 917−918; (c) R. N. Grimes, Chem. Rev. 92 (1992) 251−268; (d) A. K. Saxena, N. S. Hosmane, Chem. Rev. 93 (1993) 1081−1124.

7) (a) J. W. Lauher, M. Elian, R. H. Summerville, R. Hoffmann, J. Am. Chem. Soc. 98 (1976) 3219−3224; (b) V. Beck, D. O'Hare, J. Organomet. Chem. 689 (2004) 3920−3938; (c) D. A. Loginov, D. V. Muratov, A. R. Kudinov, Russ. Chem. Bull. 57 (2008) 1−7.

8) (a) H. Werner, Angew. Chem., Int. Ed. Engl. 16 (1977) 1−9; (b) T. Chivers, I. Manners, Inorganic rings and polymers of the p-block elements: from fundamentals to applications, RSC Publishing, Cambridge, 2009.

9) (a) H. Werner, A. Salzer, Inorg. Met.-Org. Chem. 2 (1972) 239−248; (b) A. Salzer, H. Werner, Angew. Chem., Int. Ed. Engl. 11 (1972) 930−932; (c) E. Schumacher, R. Taubenest, Helv. Chim. Acta 47 (1964) 1525−1529.

10) (a) D. C. Beer, V. R. Miller, L. G. Sneddon, R. N. Grimes, M. Mathew, G. J. Palenik, J. Am. Chem. Soc. 95 (1973) 3046−3048; (b) R. N. Grimes, Acc. Chem. Res. 11 (1978) 420−427; (c) R. N. Grimes, Coord. Chem. Rev. 28 (1979) 47−96.

11) (a) T. J. Colacot, N.S. Hosmane, Z. Anorg. Allg. Chem. 631(2005) 2659−2668; (b) D. A. Loginov, V. E. Konoplev, J. Organomet. Chem. 867 (2018) 14–24.

12) A. K. Kandalam, B. Kiran, P. Jena, J. Phys. Chem. C 112 (2008) 6181–6185.

13) (a) W. Siebert, Angew. Chem. Int. Ed Engl. 24 (1985) 943–958; b) W. Siebert, Pure & Appl. Chem. 60 (1988) 1345–1348; (b) T. Kuhlmann, S. Roth, J. Roziere, W. Siebert, U. Zenneck, Synthetic Metals 19 (1987) 757–762.

14) A. Thakur, K. K. V. Chakrahari, B. Mondal, S. Ghosh, Inorg. Chem. 52 (2013) 2262−2264.

15) (a) B. Mondal, K. Pal, B. Varghese, S. Ghosh, Chem. Commun. 51 (2015) 3828−3831; (b) B. Mondal, M. Bhattacharyya, B. Varghese, S. Ghosh, Dalton Trans. 45 (2016) 10999−11007.

16) S. Ghosh, A. M. Beatty, T. P. Fehlner, J. Am. Chem. Soc. 123 (2001) 9188−9189.

17) R. Bag, R. Prakash, S. Saha, T. Roisnel, and S. Ghosh, Inorg. Chem. 60 (2021) 3524−3528.

18) S. Aldridge, T. P. Fehlner, M. Shang, J. Am. Chem. Soc. 119 (1997) 2339–2340.

19) (a) A. S. Weller, M. Shang, T. P. Fehlner, Organometallics 18 (1999) 53−64; (b) R. Bag, S. Kar, S. Saha, S. Gomosta, B. Raghavendra, T. Roisnel, S. Ghosh, Chem. Asian J. 15 (2020) 780–786.

20) K. Wade, J. Chem. Soc. D Chem. Commun. 15 (1971) 792-793; b) D. M. P. Mingos, Nat. Phys. Sci. 236 (1972) 99−102.

21) (a) M. Elian, M. M.-L Chen, D. M. P. Mingos, R. Hoffmann, Inorg. Chem. 15 (1976) 1148−1155; (b) R. Hoffmann, Angew. Chem. Int. Ed. 21 (1982) 711−724.

22) (a) J.-F. Halet, Coord. Chem. Rev. 143 (1995) 637−678; (b) J.-F. Halet, R. Hoffmann, J.-Y Saillard, Inorg. Chem. 24 (1985) 1695−1700.

23) (a) T. L. Venable, E. Sinn, R. N. Grimes, Inorg. Chem. 21 (1982) 904−908; (b) H. Yan, A. M. Beatty, T. P. Fehlner, Organometallics 21 (2002) 5029−5037; (c) R. Borthakur, R. Prakash, P. Nandi, S. Ghosh, J. Organomet. Chem. 825−826 (2016) 1−7; (d) D. K. Roy, R. S. Anju, B. Varghese, and S. Ghosh, Organometallics 32 (2013) 1964−1970; (e) D. K. Roy, R. Jagan, S. Ghosh, J. Organomet. Chem. 772-773 (2014) 242−247.

24) (a) T. P. Fehlner, J.-F. Halet, J.-Y. Saillard, Molecular Clusters. A Bridge to Solid State Chemistry. Cambridge University Press, Cambridge, Grande-Bretagne, 2007; (b) K. Geetharani, B. S. Krishnamoorthy, S. Kahlal, S. M. Mobin, J.-F. Halet, S. Ghosh, Inorg. Chem. 51 (2012) 10176–10184; (c) K. K. V. Chakrahari, D. Sharmila, S. K. Barik, B.

Mondal, B. Varghese, S. Ghosh, J. Organomet. Chem. 749 (2014) 188−196; (e) D. K. Roy, B. Mondal, R. S. Anju, S. Ghosh, Chem. Eur. J. 21 (2015) 3640–3648; (f) B. S. Krishnamoorthy, A. Thakur, K. K. V. Chakrahari, S. K. Bose, P. Hamon, T. Roisnel, S. Kahlal, S. Ghosh, J-F. Halet, Inorg. Chem. 51 (2012) 10375-10383; (g) S. Sahoo, K. H. K. Reddy, R. S. Dhayal, S. M. Mobin, V. Ramkumar, E. D. Jemmis, S. Ghosh, Inorg. Chem. 48 (2009) 6509–6516.

25) (a) S. Aldridge, H. Hashimoto, K. Kawamura, M. Shang, T. P. Fehlner, Inorg. Chem. 37 (1998) 928−940; (b) H. Hashimoto, M. Shang, T. P. Fehlner, J. Am. Chem. Soc. 118 (1996) 8164−8165; (c) B. Mondal, R. Bag, T. Roisnel, S. Ghosh, Inorg. Chem. 58 (2019) 2744−2754; (d) R. Bag, S. Saha, R. Borthakur, B. Mondal, T. Roisnel, V. Dorcet, J.-F Halet, S. Ghosh, Inorganics 7 (2019) 27.

26) S. Ghosh, M. Shang, T. P. Fehlner, J. Am. Chem. Soc. 121 (1999) 7451−7452.

27) B. Le Guennic, H. Jiao, S. Kahlal, J.-Y Saillard, J.-F. Halet, J.-F., S. Ghosh, M. Shang, A. M. Beatty, A. L. Rheingold, T. P. Fehlner, J. Am. Chem. Soc. 126 (2004) 3203−3217.

28) K. Wiberg, Tetrahedron 24 (1968) 1083–1096.

29) (a) A. E. Reed, L. A. Curtiss and F. Weinhold, Chem. Rev. 88 (1988) 899–926; (b) F. Weinhold, C. R. Landis, Valency and Bonding: A Natural Bond Orbital Donor-Acceptor Perspective, Cambridge University Press, Cambridge, UK, 2005; (c) R. B. King, Inorg. Chem., 38 (1999) 5151–5153; (d) R. B. King, Inorg. Chim. Acta 300 (2000) 537–544.

30) (a) R. S. Dhayal, S. Sahoo, V. Ramkumar, S. Ghosh, J. Organomet. Chem. 694 (2009) 237–243; (b) M. L. H. Green, J. D. Hubert, P. Mountford 12 (1990) 3793–3800; (c) M. Kaushika, A. Singh, M. Kumar, Eur. J. Chem. 3 (2012) 367–394.

31) G. E. Ryschkewitsch, K. C. Nainan, Inorg. Synth. 15 (1974) 113–114.

32) M. J. Frisch, G. W. Trucks, H. B. Schlegel, G. E. Scuseria, M. A. Robb, J. R. Cheeseman, G. Scalmani, V. Barone, G. A. Petersson, H. Nakatsuji, X. Li, M. Caricato, A. V. Marenich, J. Bloino, B. G. Janesko, R. Gomperts, B. Mennucci, H. P. Hratchian, J. V. Ortiz, A. F. Izmaylov, J. L. Sonnenberg, D. Williams-Young, F. Ding, F. Lipparini, F. Egidi, J. Goings, B. Peng, A Petrone, T. Henderson, D. Ranasinghe, V. G. Zakrzewski, J. Gao, N. Rega, G. Zheng, W. Liang, M. Hada, M. Ehara, K. Toyota, R. Fukuda, J. Hasegawa, M. Ishida, T. Nakajima, Y. Honda, O. Kitao, H. Nakai, T. Vreven, K. Throssell, J. A. Jr. Montgomery, J. E. Peralta, F. Ogliaro, M. J. Bearpark, J. J. Heyd, E. N. Brothers, K. N. Kudin, V. N. Staroverov, T. A. Keith, R. Kobayashi, J. Normand, K. Raghavachari, A. P. Rendell, J. C. Burant, S. S. Iyengar, J. Tomasi, M. Cossi, J. M. Millam, M. Klene, C. Adamo, R. Cammi, J. W. Ochterski, R. L. Martin, K. Morokuma, O. Farkas, J. B. Foresman, D. J. Fox, Gaussian, Inc., Wallingford CT, 2016.

33) C. Lee, W. Yang, R. G. Parr, Phys. Rev. B: Condens. Matter Mater. Phys. 37 (1988) 785–789.

34) T. Lu, F. Chen, J. Comput. Chem. 33 (2012) 580–592.

35) G. M. Sheldrick, Acta Cryst A 71 (2015) 3–8.

36) G. M. Sheldrick, Acta Cryst. C 71 (2015) 3–8.

37) O. V. Dolomanov, L. J. Bourhis, R. J. Gildea, J. A. K. Howard, H. Puschmann, J. Appl. Cryst. 42 (2009) 339–341.

Scheme 1. Synthesis of **1**.

Scheme 2. Synthesis of the tungstaborane clusters **2** and **3**.

Fig. 1. Selected bond lengths (Å) and bond angles (°) of **2**: W1-Co1 2.8153(18), W1-Co2 2.7446(17), W2-Co1 2.7479(17), W2-Co2 2.8037(19), Co1-Co2 2.525(2), W1-B1 2.31(2), W1-B2 2.30(2), W2-B3 2.26(3), Co1-B1 2.10(2), Co1-B3 2.02(2), Co2-B2 2.13(2), Co2-B3 2.03(3), B1-B2 1.77(3), B1-B3 1.69(3), B2-B3 1.70(3); Co1-W2-Co2 54.09(5), W1-Co2-W2 123.61(5), B2-W1-B1 45.1(8), B1-W1-Co2 71.5(6), B1-Co1-B3 48.5(9), B1-Co1-Co2 79.4(7), B3-Co1-W1 79.1(8), B2-Co2-Co1 80.0(6), B1-B3-B2 62.8(15).

Fig. 2. Selected bond lengths (Å) and bond angles (°) of **3** (molecule B): W3-W4 2.8706(16), Co3-Co4 2.432(5), W3-Co3 2.725(4), W3-Co4 2.707(4), W4-Co3 2.714(4), W4-Co4 2.740(4), W3-B4 2.29(3), W3-B5 2.21(3), W3-B6 2.34(3), W4-B4 2.24(3), W4-B5 2.22(3), W4-B6 2.28(3), Co3-B4 2.04(3), B4-B5 1.75(4), B5-B6 1.76(5); B5-W3-B4 45.7(11), B4-W3-B6 84.3(11), B5-W3-Co4 108.5(8), B5-W3-W4 49.8(8), Co4-W3-W4 58.74(9), B4-W4-W3 51.5(8), B5-B4-Co3 132(2), B4-B5-B6 125(2).

Fig. 3. DFT-optimized structure of **1'**.

Fig. 4. Frontier molecular diagrams and HOMO-LUMO gaps (eV) of **1′**, **I′** and **3′**.

Chart 1. Examples of capped octahedral metallaborane clusters reported in the literature.

Table 1. Avg. M-M, M-B and B-B bond lengths of **2** and similar compounds.

Table 2. Avg. M-M, M-B and B-B bond lengths of **3** and similar compounds.

Scheme 1

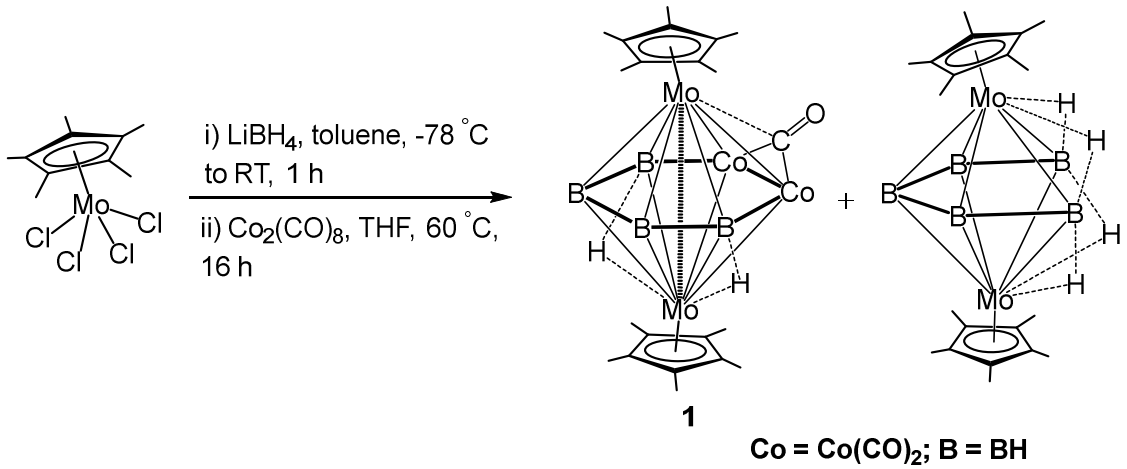

Scheme 2

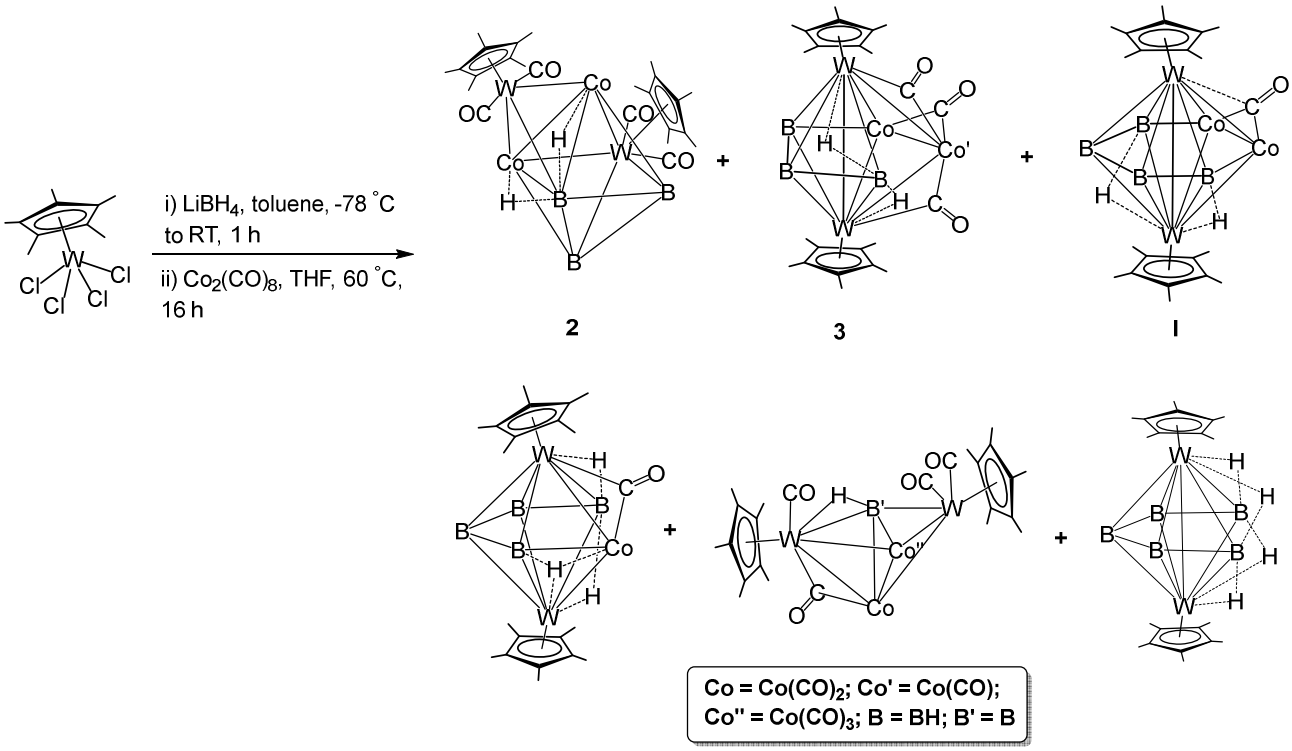

Fig. 1.

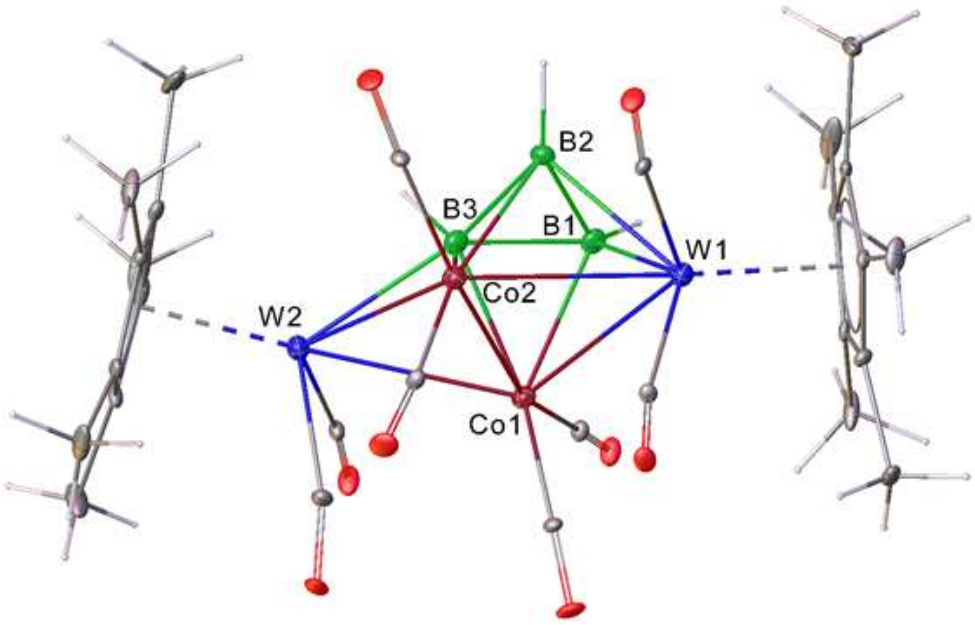

Fig. 2.

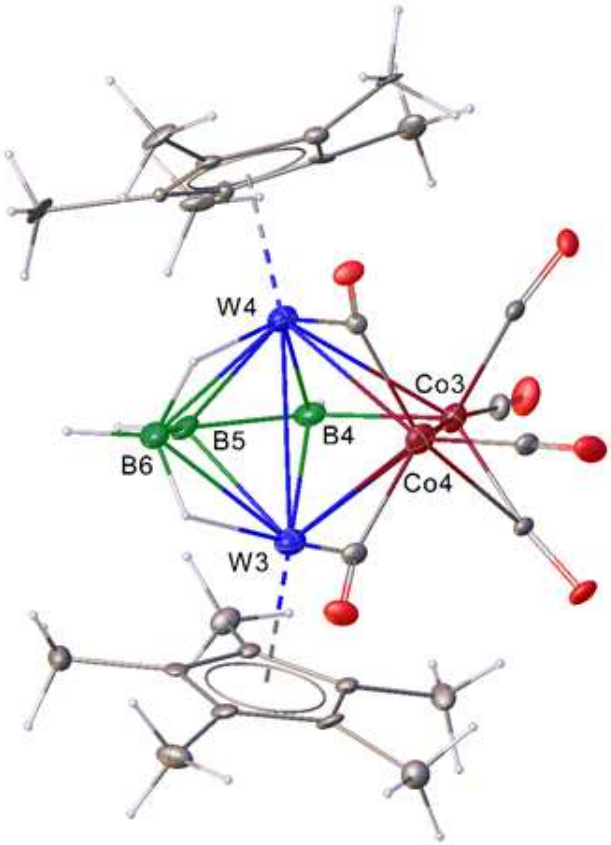

Fig. 3.

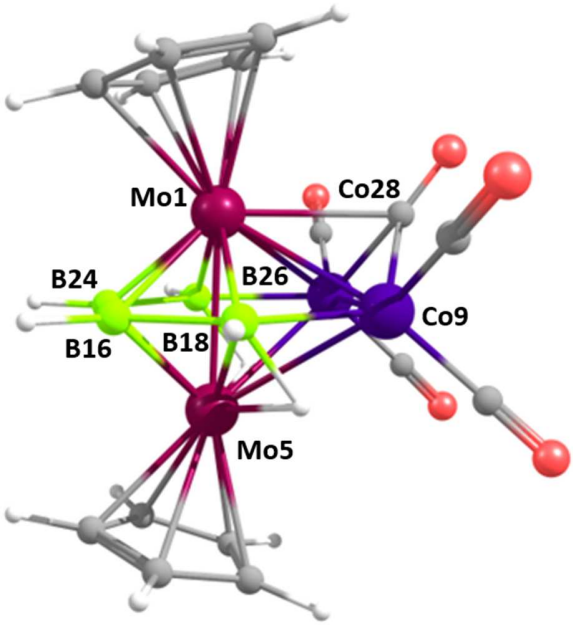

Fig. 4.

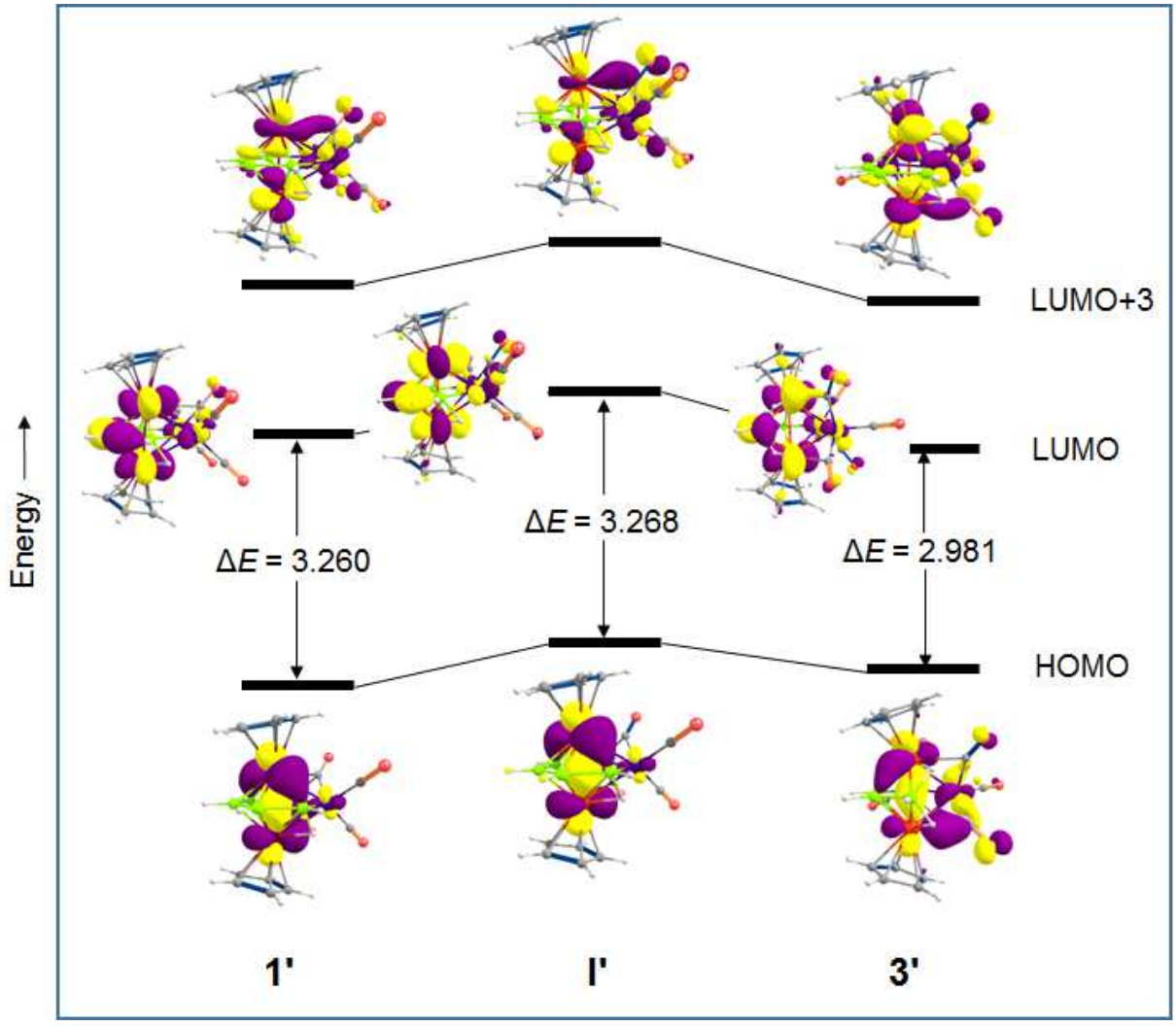

Chart 1

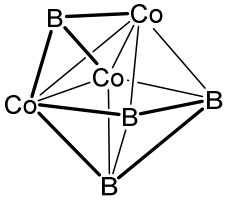

$[(Cp^*Co)_3B_4H_4]$

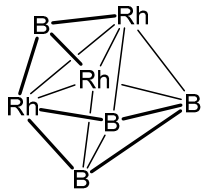

$[(Cp^*Rh)_3B_4H_4]$

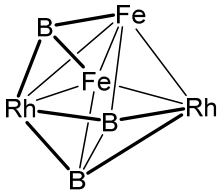

$[(Cp^*Rh)_2B_3H_3\{Fe(CO)_3\}_2]$

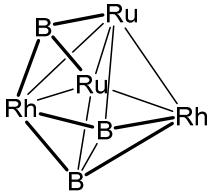

$[(Cp^*Rh)_2B_3H_3\{Ru(CO)_3\}_2]$

Table 1.

Compound	sep count	*d*(M-M) (Å)	*d*(M-B) (Å)[a]	*d*(B-B) (Å)[a]
$[(Cp^*Co)_3B_4H_4]$[23a]	7	2.50	2.00	1.70
$[(Cp^*Rh)_3B_4H_4]$[23b]	7	2.67	2.11	1.73
$[(Cp^*Ir)_3B_4H_4]$[23c]	7	2.70	2.08	1.70
$[(Cp^*Rh)_2B_3H_3\{Fe(CO)_3\}_2]$[23d]	7	2.63	2.09	1.80
$[(Cp^*Rh)_2B_3H_3\{Ru(CO)_3\}_2]$[23e]	7	2.77	2.15	1.80
$[\{Cp^*W(CO)_2\}_2(\mu\text{-}H)_2B_3H_3Co_2(CO)_4]$ (**2**)	8	2.70	2.22	1.74

Table 2.

Compound	sep count	*d*(M-M) (Å)	*d*(M-B) (Å)[a]	*d*(B-B) (Å)[a]
$[(Cp^*Cr)_2Co(CO)_3B_4H_7]$[25a]	6	2.69	2.13	1.69
$[(Cp^*Cr)_2B_4H_8Fe(CO)_3]$[25b]	6	2.71	2.15	1.72
$[(Cp'Mo)_2(\mu\text{-}H)_4B_5H_5]$[b] [18]	6	2.81	2.26	1.73
$[(Cp^*W)_2(\mu\text{-}H)_4B_5H_5]$ [19]	6	2.82	2.26	1.71
$[(Cp^*Mo)_2B_5H_9Fe(CO)_3]$ [25a]	7	2.94	1.75	1.76
$[(Cp^*Mo)_3B_4H_4(\mu\text{-}CO)_2(\mu\text{-}H)_2(\mu_3\text{-}H)]$ [25c]	6	2.91	2.28	1.72
$[(Cp^*Mo)_2B_4H_4(\mu\text{-}H)_2(\mu_3\text{-}H)_2W(CO)_4]$ [25c]	6	2.91	2.24	1.72
$[(Cp^*Mo)_2B_4H_4(\mu\text{-}H)_2W(CO)_5]$ [25c]	6	2.91	2.24	1.73
$[(Cp^*W)_2B_4H_4Mo(CO)_4(\mu\text{-}H)_2(\mu_3\text{-}H)_2]$ [25d]	6	2.97	2.32	1.72
$[(Cp^*W)_2B_3H_3Co_2(CO)_4(\mu\text{-}CO)_2(\mu\text{-}H)_2]$ (**3**)	6	2.87	2.25	1.75

[a] Average distance, [b] Cp' = η^5-MeC_5H_4.